

Evaluating the cascading impacts of sea level rise and coastal flooding on emergency response spatial accessibility in Lower Manhattan, New York City

Jie Yin^{1,2,3*}, Dapeng Yu⁴, Ning Lin³, Robert L. Wilby⁴

1 Key Laboratory of Geographic Information Science (Ministry of Education), East China Normal University, China

2 School of Geographic Sciences, East China Normal University, China

3 Department of Civil and Environmental Engineering, Princeton University, US

4 Centre for Hydrological and Ecosystem Science, Department of Geography, Loughborough University, UK

Abstract: This paper describes a scenario-based approach for evaluating the cascading impacts of sea level rise (SLR) and coastal flooding on emergency responses. The analysis is applied to Lower Manhattan, New York City, considering FEMA's 100- and 500-year flood scenarios and New York City Panel on Climate Change (NPCC2)'s high-end SLR projections for the 2050s and 2080s, using the current situation as the baseline scenario. Service areas for different response timeframes (3-, 5- and 8-minute) and various traffic conditions are simulated for three major emergency responders (i.e. New York Police Department (NYPD), Fire Department, New York (FDNY) and Emergency Medical Service (EMS)) under normal and flood scenarios. The modelling suggests that coastal flooding together with SLR could result in proportionate but non-linear impacts on emergency services at the city scale, and the performance of operational responses is largely determined by the positioning of emergency facilities and the functioning of traffic networks. Overall, emergency service accessibility to the city is primarily determined by traffic flow speed. However, the situation is expected to be further aggravated during coastal flooding, with is set to increase in frequency and magnitude due to SLR.

Keywords: Emergency response; coastal flooding; sea level rise; Lower Manhattan

1 Introduction

Sea level rise (SLR) is among the most certain consequences of anthropogenic climate change, with significantly adverse effects on coastal settlements and ecosystems through permanent inundation of low-lying waterfront areas and by aggravating coastal flooding over a larger inland region (Hu and Deser, 2012; Nicholls and Cazenave, 2010). Tide gauge records show that global mean sea level rose by an average rate of 1.6 to 1.9 mm/year over the twentieth century (Hay et al., 2015), and CMIP5 climate models project a rise of 0.26 to 0.82 m in mean sea level rise by the end of 21st century (IPCC, 2012). Regional rates of sea level change vary from the global mean, due to local changes in oceanic circulation, variations in ocean temperature and salinity, vertical land movements, and static equilibrium processes (Mitrovica et al., 2001; Levermann et al., 2005; Kopp et al., 2014). For example, sea level has risen by 3 mm/year since 1900 in the vicinity of New York City (NYC) with only 60% of the observed SLR driven by climate-related factors and the remaining 40% caused by local factors (such as land subsidence). Climate model projections suggest a further rise of up to 1.9 m by 2100 (Peltier, 2004; Engelhart and Horton, 2012; Horton et al., 2015).

43 The effect of SLR on coastal flooding is well-documented globally. In the New York Harbor region SLR has
44 significantly increased the frequency and/or intensity of storm tide flooding, with eight of the largest twenty extreme
45 water levels occurring after 1990 (Talke et al., 2014). Hurricane Sandy generated the highest storm tide in the city's
46 history and the most destructive flooding over NYC, resulting in considerable losses (45 deaths and more than \$20
47 billion loss) and extensive indirect impacts (e.g. interruption of citywide infrastructure and public services) (NYC
48 OEM, 2014). Towards the end of the 21st century, even if storm climatology does not change, the current 100-year
49 flood for the city is projected to occur 2 to 4 times more often under the middle range of local NYC SLR estimates
50 (Horton et al., 2015) and the current Sandy-like flood is projected to occur over 4 times more often (Lin et al., 2016)
51 due to SLR. Hence, without further coastal adaptations, the city is expected to experience increasing flood risks under
52 a changing climate (Aerts et al., 2014; Hallegatte et al., 2013).

53

54 In response to evolving coastal flooding, local governments are required to provide efficient risk management to
55 meet legislative requirements (e.g. response time for high priority incidents) (Rosenzweig and Solecki, 2014).
56 Emergency services are in the front-line of the operational response. In the United States, emergency responses (such
57 as search, rescue and emergency medical services (EMS)) to hazards operating at local (city or community) scale are
58 mostly provided by a division of the Police and/or Fire Departments with the responsibility to dispatch emergency
59 resources to save lives and reduce damages as soon as possible during an event. During and after Hurricane Sandy,
60 there was a 37-fold increase in water rescues compared to the normal conditions. The New York City Police
61 Department (NYPD) and Fire Department of the City of New York (FDNY) rescued more than 2,200 people from
62 the rising water of the storm and performed grid searches of more than 31,000 homes and businesses once floodwaters
63 receded (NYC Mayor's Office, 2012).

64

65 There has been limited research into the cascading impacts of flood-induced road network failures on emergency
66 service provisions in a changing climate. A few studies focus on the development and application of high resolution
67 coastal flood models (e.g. Bates et al. 2005; Blumberg et al. 2015; Wang et al. 2014; Ramirez et al. 2016); others
68 address the impacts of flooding on surface transportation system (e.g. Chang et al. 2010). For example, Gil &
69 Steinbach (2008) evaluated the indirect consequences of flooding on an urban street network by removing flooded
70 road sections from the transport system. Yin et al. (2016a) used a high resolution 2D inundation model and a flood
71 depth-dependent measure (30 cm) to examine the accessibility losses of an intra-urban road network under various
72 flood magnitudes. Identification of flood hotspots and extent of disrupted road network enables evaluation of impacts
73 on emergency responders' performance. More recently, a framework for incorporating flood modelling with
74 accessibility mapping for emergency responders has been developed by Coles et al. (2017), and demonstrated in the
75 City of York with pluvial and fluvial events occurred in the city. Similarly, Green et al. (2017) evaluated the spatial
76 coverage of emergency responders during pluvial and fluvial flood risks with various return periods for the City of
77 Leicester, UK. Both studies focus on the accessibility of emergency responders to vulnerable populations (e.g. care
78 homes) during flood events and within mandatory timeframes (8 minutes for Ambulance Service and 10 minutes for
79 Fire & Rescue Service in the UK).

80

81 Although there is no federal or state standard for emergency response time in the U.S., some requirements do exist
82 in different communities. For example, EMS is mandated by the NYC to meet an average 10-minute response time
83 on emergency calls. According to 911 performance statistics collected for NYC¹ since November 2012, the majority
84 of the End-to-End response time (including pickup, dispatch, processing and travel) was spent on traveling (3 to 9

¹ <http://www.nyc.gov/html/911reporting/html/reports/end-to-end.shtml>

85 minutes). During coastal flood emergencies, waterfront road networks can be affected by inundation, leading to
86 significant travel delays (i.e. longer response times) and even widespread disruption of emergency services. The
87 efficiency of coastal flood emergency response largely depends on the functioning of transport network in the coastal
88 floodplain. For instance, storm surge associated with hurricane Sandy flooded large proportions of the coastal road
89 network of NYC, especially in the Manhattan area, delaying emergency fire response in Queens (FEMA, 2012).

90
91 In this paper, we develop a scenario-based approach to quantify the impacts of SLR and coastal flooding on urban
92 emergency response times using hydrodynamic modeling and GIS-based network analysis. Lower Manhattan
93 (downtown and midtown, south of 57th Street), the Central Business District (CBD) of NYC, was used as a case
94 study as it is highly vulnerable to coastal flooding induced by storm surge, which is expected to increase due to the
95 change of storm climatology, in a magnitude comparable to the projected sea-level rise (SLR) (Lin et al., 2012). For
96 example, the combined effects of storm climatology change and a 1-m SLR may result in the current NYC 100-year
97 surge flooding to occur every 3-20 years and the 500-year flooding to occur every 25-240 years, by the end of the
98 century (Lin et al., 2012). We begin by exploring the spatial-temporal characteristics of coastal flooding with rapid
99 SLR over the coming decades. We then use the flood maps generated to investigate accessibility of the city by
100 emergency services and to identify vulnerable facilities that lie within the inundated areas. Section 2 introduces the
101 materials and methods, including data, coastal flood modeling and emergency service evaluation; Section 3 presents
102 the results and discusses the key findings; finally, Section 4 provides the conclusions and offers suggestions for
103 further research.

104

105 **2 Materials and methods**

106

107 **2.1 Data and processing**

108

109 2.1.1. Flood scenarios

110

111 Coastal flood scenarios were designed to evaluate the potential impacts of flooding on emergency service response.
112 We apply FEMA’s 100-year and 500-year coastal flood estimates for NYC to establish the current and baseline flood
113 scenarios. Based on the frequency analysis undertaken by FEMA flood insurance study in 2012 (FEMA, 2012), the
114 flood heights above NAVD 88 Datum for 1 in 100- and 500-year events along the NYC floodplain-sea boundary are
115 used. To account for the effect of SLR, projected SLRs (see below) are linearly added to these baseline floods to
116 create the flood scenarios for the 2050s and 2080s. Here we do not consider possible changes in the storm climatology
117 in the future climate (Lin et al., 2012 and 2016).

118

119 2.1.2 Local sea level rise

120

121 In this study, we apply NPCC2’s SLR projection for NYC, which were developed based on a seven-component
122 approach (Horton et al., 2015), including relative ocean height, local fingerprint associated with the ocean’s responses
123 to ice mass loss, and land height change terms (NPCC2, 2013). The report is widely regarded as the most systematic
124 study of SLR in NYC and has been officially adopted by local government in coastal resilience planning. Compared
125 to other SLR studies (e.g. Kopp et al., 2014), the NPCC2’s results show a wider range primarily due to the different
126 sources of components considered, assumptions made and distributions assumed. To account for plausible yet
127 extreme scenarios, high-end estimates (i.e. 90th percentiles of model-based distributions) of NPCC2’s SLR
128 projections were derived for the 2050s (0.76 m) and 2080s (1.47 m), relative to the 1971-2000 baseline.

129

130 2.1.3 Topography dataset

131

132 Floodplain topography is available for NYC in the form of a Digital Elevation Model (DEM). The data were acquired
133 by the NYC Department of Environmental Protection and the Department of Information Technology &
134 Telecommunications in 2012 using Light Detection and Ranging (LiDAR) technology. The DEM was constructed
135 from LiDAR point cloud with a horizontal resolution of 30 cm and a vertical accuracy of $\pm 10\sim 20$ cm. In this study,
136 a “bare earth” topography based on North American Vertical Datum of 1988 (NAVD 88) was produced by removing
137 non-topographic features (e.g. trees, cars and buildings). Building representation in urban hydrodynamic model is an
138 active research field as buildings represent barriers to flow and reduce the area available for water storage (e.g. [Yu
139 and Lane 2006b](#); [Fewtrell et al 2008](#); [Neal et al. 2011](#)). The impact of four treatment methods for building topography
140 (building resistance, building block, building hole, and building porosity) has been investigated using a 2D flood
141 inundation model ([Schubert and Sanders, 2012](#)). Results suggest that all four approaches support sufficiently accurate
142 flood extent and stream flow prediction. The best method for a particular application depends on data availability,
143 modeling objectives and user tolerances for pre-processing and run-time costs. Considering the size of the simulation
144 domain and focus of the paper, building effects were modeled in our analysis using building resistance method, i.e.
145 relatively high Manning coefficient. To reduce the computational costs, the 0.3 m LiDAR DEM was further
146 resampled to a 6 m grid resolution using bilinear interpolation method, resulting in a DEM sufficiently fine to
147 represent primary urban surface features (e.g. roads). Consequently, the simulation domain of the Lower Manhattan
148 consists of 1000×1300 grids, or 1.3 million cells.

149

150 2.1.4 Road network and facilities

151

152 The most recent (updated in August 2016) GIS dataset of city facilities and a single line street base map (i.e. LION)
153 were obtained from the NYC Open Data Portal². Locations of critical emergency responders were identified from
154 the city facility layer, including 30 fire houses (FS), 11 police stations (PS), and 2 EMS centers. Locations of
155 vulnerable healthcare facilities include nursing homes, hospitals, hospices, and adult day care facilities were also
156 derived from the dataset. City streets and traffic directions were extracted from LION. Current speed limits (i.e. 40
157 mph for F.D.R. (Franklin D. Roosevelt East River Drive), 35 mph for West Street, 11 and 12 Avenue, and 20~25
158 mph for the other roadways) were collected and assigned to each road sections in Lower Manhattan. Traffic signals
159 and other driving regulations, which emergency vehicles are exempt from (e.g. one way and U-turn), were not
160 considered. A transport network dataset was then created using the default turn restrictions in ArcGIS10.2.

161

162 2.2 Coastal flood modeling

163

164 A simplified 2D flood inundation model (FloodMap-Inertial) – a revised version of an earlier diffusion-based model
165 (FloodMap, [Yu and Lane 2006a, b](#)) – was used to simulate the hydrodynamics of coastal flooding. The model has
166 been calibrated for the NYC using the 2012 Hurricane Sandy event, against the highest water levels obtained from
167 USGS HWMs (High Water Marks), deployed along the NYC coast prior to storm landfall. ([Yin et al., 2016b](#)). The
168 simplified 2D solutions have been shown to perform as well as full 2D models for the treatment of coastal flooding,
169 but at much lower computational cost ([Bates et al., 2005](#)). The module used here solves the inertial form of the 2D
170 shallow water equations in a raster-based environment. Surface flood routing takes the same form as the inertial

² <http://www1.nyc.gov/site/planning/data-maps/open-data.page>

171 algorithm of Bates et al. (2010), but with a different approach to time step calculation, which forward calculates the
 172 optimal time step for the next iteration rather than using the time step calculated in the current iteration for the next.
 173 The details of the model structure have been presented in Yu and Lane (2011), and the key features of the model
 174 structure are presented below. The momentum equation in the Saint-Venant equations without the convective
 175 acceleration term takes the form:

$$176 \quad \frac{\partial q}{\partial t} + \frac{gh\partial(h+z)}{\partial x} + \frac{gn^2q^2}{R^{4/3}h} = 0$$

177 where q is the flow per unit width, g is the acceleration due to gravity, R is the hydraulic radius, z is the bed elevation,
 178 h is the water depth, and n is the Manning's roughness coefficient. R can be approximated with h for wide and shallow
 179 flows. Discretizing the equation with respect to time gives:

$$180 \quad \frac{q_{t+\Delta t} - q_t}{\Delta t} + \frac{gh_t\partial(h+z)}{\partial x} + \frac{gn^2q_t^2}{h_t^{7/3}} = 0$$

181 where one of the q_t in the friction term can be replaced by $q_{t+\Delta t}$, resulting in the explicit expression of the flow at the
 182 next time step:

$$183 \quad q_{t+\Delta t} = \frac{q_t - gh_t\Delta t\left(\frac{\partial(h+z)}{\partial x}\right)}{(1 + gh_t\Delta t n^2 q_t / h_t^{10/3})}$$

184 Flows in the x and y directions are decoupled and take the same form. Discharge is evaluated at cell edges and depth
 185 at the cell centre. To maintain model stability and minimize numerical diffusion, the Forward Courant-Freidrich-
 186 Levy Condition (FCFL) approach described in Yu and Lane (2011) for the diffusion-based version of FloodMap is
 187 used in the inertial model to calculate the time step:

$$188 \quad \Delta t \leq \min\left(\frac{wd_id_jn}{d_i^{1.67}(S_i)^{1/2} + d_j^{1.67}(S_j)^{1/2}}\right)$$

189 where w is the cell size, d_i and d_j are the effective water depths; S_i and S_j are water surface slopes; and i and j are the
 190 indices for the flow direction in the x and y directions, respectively. The effective water depth is defined as the
 191 difference between the higher water surface elevation and the higher bed elevation of two cells that exchange water.
 192 The minimum time step that satisfies the FCFL condition for all wet cells is used as the global time step for this
 193 iteration. This approach does not require the back calculation of Courant number as the time step is calculated based
 194 on the CFL condition that satisfies every wet grid cell for the current iteration. The universal time step calculated
 195 with FCFL may need to be scaled further by a coefficient, with a value between 0 and 1, as the FCFL condition is not
 196 strictly the right stability criteria for an inertial system. A scaling factor in the region 0.5 to 0.8 was found to yield a
 197 stable solution in previous studies – a scaling factor of 0.7 was used herein for all simulation. Calibration and
 198 validation of the model have been conducted for the study area in Yin et al. (2016b). A relatively high floodplain
 199 roughness value (Manning's $n=0.06$) was used in the present simulations to represent the effect of urban features (e.g.
 200 buildings) on flow routing.

201
 202 To apply FloodMap for inundation simulation, we convert the static flood scenarios to dynamic boundary conditions,
 203 by scaling Hurricane Sandy's stage hydrograph. Specifically, the hourly water level recorded at the Battery gauge
 204 station during Hurricane Sandy was scaled according to each flood scenario. A constant tidal cycle with two rising
 205 phases and two falling limbs, similar to that during Hurricane Sandy, was applied. The stage hydrograph was scaled
 206 for and applied to each of the 23 coastline sections (defined by the FEMA flood maps) in the study area to drive the
 207 inundation analysis. The baseline 2012 tidal hydrograph was scaled up proportionally from the onset to the peak

208 where the projected SLR heights are imposed.

209

210 **2.3 Emergency response evaluation**

211

212 2.3.1 Defining flood restriction

213

214 Regular vehicles such as compact or full size cars should avoid travelling through flood water higher than 25-35 cm
215 as these are the heights of their exhaust pipes, water above which may cause loss of control for the moving vehicles.
216 In many cities around the world (e.g. Shanghai), floodwater depth ≥ 25 cm was adopted as a critical threshold for
217 road closures. Previous studies in the UK (e.g. [Green et al., 2017](#); [Coles et al., 2017](#)) used 25 cm as a threshold of
218 blockage to emergency vehicles (Ambulance; Fire & Rescue), based on the understanding that the depth of extensive
219 waterbody on the road may be difficult to determine any submerged objects or features (such as open manhole covers)
220 that may pose unforeseen threats, even to emergency vehicles. Moreover, floodwater velocity is known to affect road
221 infrastructures and vehicles ([Kreibich et al., 2009](#)). For example, [Tingsanchali \(1996\)](#) indicated that if the floodwater
222 reaches an average depth of 0.5 m, a flow velocity of 1.0 m/s is the tipping point for vehicle instability. In case of
223 higher velocity, a very shallow depth of water may raise at the contact of the vehicle, leading to unsafe wading (1.0
224 to 2.0 m/s) and even damage to light structures (over 2.0 m/s). According to NYC flood insurance study ([2013](#)), mean
225 flood velocities in Manhattan are mostly less than 2.0 m/s. Emergency responders in the NYC are equipped with
226 larger vehicles such as emergency heavy trucks which have a higher tolerance to traversing flood water. Therefore,
227 instead of using the 25 cm depth threshold used in two previous studies ([Coles et al. 2017](#); [Green et al. 2017](#)), we
228 applied a 50 cm threshold as flood restrictions to emergency vehicles and flow velocity is considered in this case.
229 Based on the coincidence of GIS roadways and water depths greater than 50 cm, street segments affected were
230 determined and treated as barriers in the road network.

231

232 2.3.2 Emergency service analysis

233

234 Polygons were created to represent the service areas that can be reached from the emergency facilities within a given
235 response time under normal (i.e. no flood) as well as disrupted conditions from different flood scenarios. The
236 emergency service coverage was calculated based on the quickest routing weighted by travel time rather than the
237 shortest path algorithm by distance from facility to destination. Using the facilities as starting points, travel impedance
238 is set to use Drive Time (Minutes) in ArcGIS Network Analyst. Three service areas lying within a 3-min, 5-min and
239 8-min drive were specified for each facility, considering that different categories of incidents require different
240 response timeframes. For example, records show that the travel time was on average about 3 ~ 5 minutes for high
241 priority incidents in NYC during 2013 and 2016 (<http://www.nyc.gov/html/911reporting/html/reports/end-to-end.shtml>). In addition, taxi GPS data since 2010 show significant traffic congestion and temporal variation with an
242 annual average travel speed of less than 10 mph in Lower Manhattan ([NYC Department of Transportation, 2016](#)).
243 To account for the effect of traffic, the sensitivity of response time to congestion was evaluated by reducing the speed
244 limits at a 5-mph interval (i.e. S1: speed limit, S2: speed limit minus 5mph, S3: speed limit minus 10mph and S4:
245 speed limit minus 15mph). Total obstruction for a prolonged period of time is an unavoidable traffic condition in
246 megacities, particularly in Lower Manhattan. In such situations, flood emergency response via road network would
247 be completely interrupted. To consider such situations, traffic modelling is needed, and real-time traffic monitoring
248 can provide live data for verifying and conditioning traffic modelling. This was not considered in our analysis.

249

250 **3 Results and discussions**

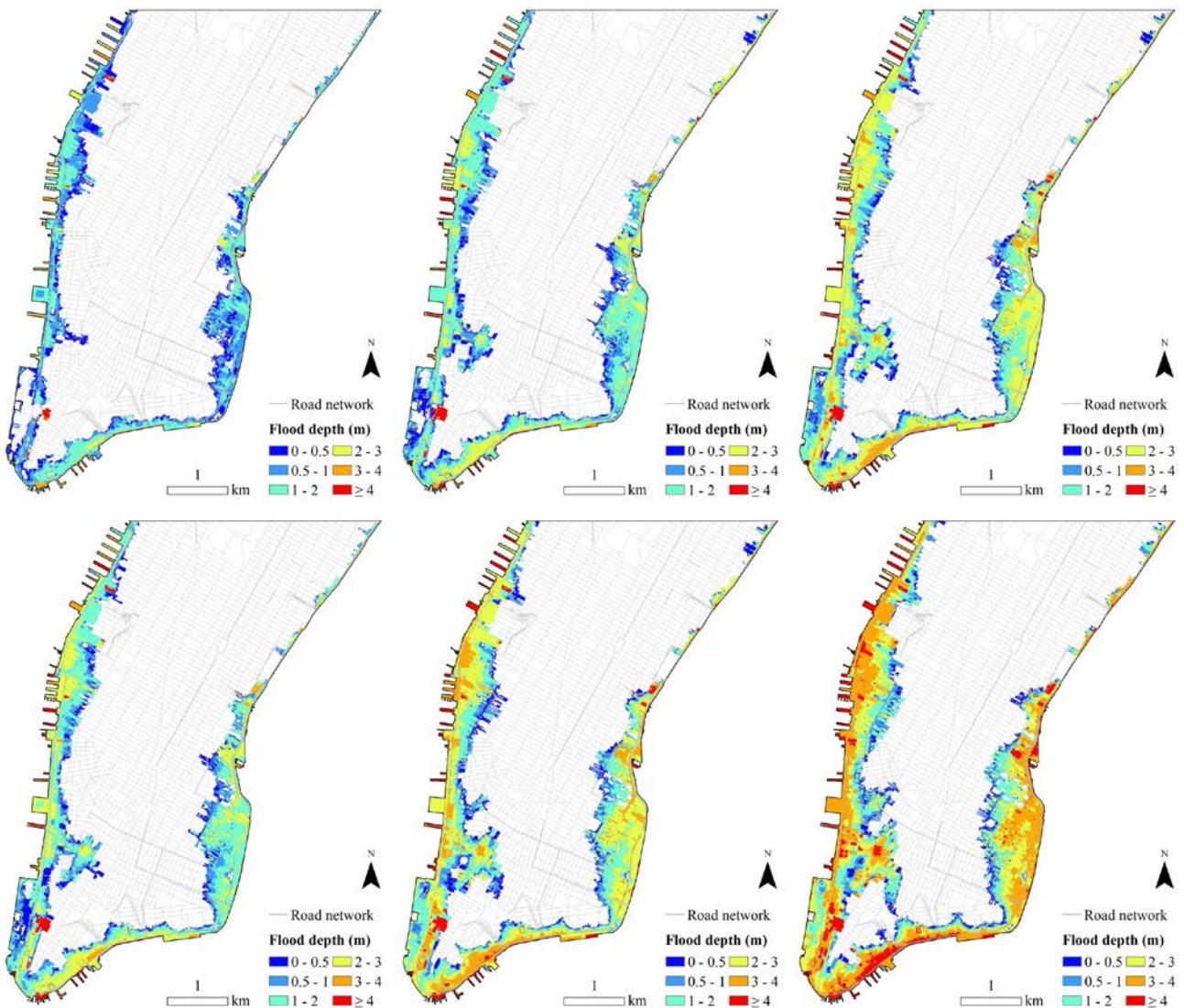
251

252

253 3.1 Coastal flood characteristics

254

255 Predicted maximum inundation depths for the 1 in 100- and 500-year coastal flood for the baseline, 2050s and 2080s
 256 scenarios are presented in Fig. 1. Comparison of the derived flood maps reveals three important findings. First, almost
 257 the entire waterfront area is subject to inundation during major flood scenarios at current and future states, due to a
 258 low-standard and fragmentary bulkhead coastal protection which is only 1.25 to 1.75 m above mean sea level in
 259 southern Manhattan (Colle et al. 2008). Second, coastal inundation extent increases proportionately with increased
 260 recurrence intervals and SLR projections over time. This can be largely attributed to the presence of lateral
 261 topographic confinement on the floodplain and thus flood water would be restricted to coastal low-lying regions,
 262 especially in the downtown area. Third, as expected, SLR significantly increases the maximum flood inundation. The
 263 magnitude of impacts, in terms of both extent and depth, depends on the rate of projected SLR. When the 0.76-m and
 264 1.47-m rise in the local sea level for the 2050s and 2080s are considered, a 35 % and 60 % increase in total inundation
 265 area is observed for the 100-year flood scenarios and a 20% and 38% increase is observed for the 500-year flood
 266 scenarios.



267

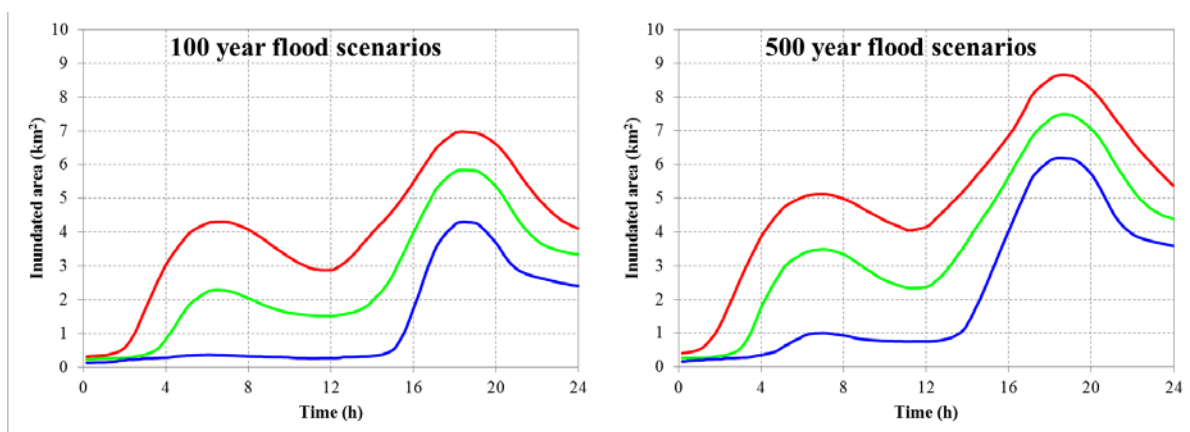
268 Fig. 1 Maximum inundation maps predicted by FloodMap for different scenarios: 100-year flood in 2012 (upper left), 100-

269 year flood in 2050s (upper middle), 100-year flood in 2080s (upper right), 500-year flood in 2012 (lower left), 500-year

270 flood in 2050s (lower middle), 500-year flood in 2080s (lower right).

271

272 In order to illustrate the temporal characteristics of coastal flood dynamics, time series of inundation areas for each
273 scenario are further explored and presented in Fig. 2. It is found that the corresponding time-area curves are in line
274 with each other. This suggests that the timing of the inundated area is synchronized with the fluctuation of storm tide,
275 expected of a relatively small domain with upward gradient further away from the shore. In each simulation, the
276 inundated extent increases rapidly during the rising phase and maximum inundation is reached shortly after the flood
277 peak, gradually decreasing afterwards as the stage subsides. Moreover, results indicate that SLR leads to
278 proportionately larger impacts on coastal flooding throughout the simulations, confirming what is found in Fig. 1.
279 With rapid rise in sea level, severe coastal inundation would occur more extensively in the low-lying floodplain, and
280 for longer durations.



281

282 Fig. 2 Time series of inundation areas for 100- and 500-year flood scenarios in 2012 (blue line), 2050s (green line) and
283 2080s (red line).

284

285 3.2 Emergency response impacts

286

287 3.2.1 Emergency services under normal conditions

288

289 Network analysis under normal conditions shows that, when no flood restrictions are in place, almost the entire area
290 is accessible within 8 minutes or less for fire and police services (Fig. 3 and Table 1). The sensitivity analysis of
291 travel speeds further reveals that fire and police emergency responses would be able to reach the majority of Lower
292 Manhattan within 3 minutes or 5 minutes even under adverse traffic conditions. For example, if emergency vehicles
293 drive at speed S4 (i.e. speed limit minus 15mph), 92% and 74% of the area would be covered within 5 minutes by
294 the fire and police services respectively. The response times presented here match well with the observations which
295 are about 3 to 5 minutes of average traveling for major FDNY (category-1, 2, 3 and 4) and NYPD (category-1 and 2)
296 emergency incident³. In addition, significant areas can be served by multiple fire and police stations during
297 emergency response. These findings suggest that fire houses and police stations are well placed throughout the region
298 with sufficient overlaps in the service area of each facility, providing a good degree of contingencies for emergency
299 response in situations where certain stations are out of action.

300

301 Table 1 Accessibility of emergency services with various travel speeds under non-flood conditions. Unit: km².

³ <http://www.nyc.gov/html/911reporting/html/reports/end-to-end.shtml>

Emergency services	EMS with various travel speeds				FDNY with various travel speeds				NYPD with various travel speeds			
	S1	S2	S3	S4	S1	S2	S3	S4	S1	S2	S3	S4
Accessible in 3 minutes	6.9 (26%)	4.25 (16%)	2.33 (9%)	1.06 (4%)	24.55 (94%)	24.41 (94%)	22.68 (87%)	14.79 (57%)	24.11 (93%)	22.58 (87%)	16.49 (63%)	7.03 (27%)
Accessible in 5 minutes	16.28 (63%)	11.59 (45%)	7.25 (28%)	3 (12%)	25 (96%)	24.95 (96%)	24.87 (96%)	23.92 (92%)	24.95 (96%)	24.88 (96%)	24.65 (95%)	19.31 (74%)
Accessible in 8 minutes	25.31 (97%)	22.32 (86%)	16.83 (65%)	9.47 (36%)	25.65 (99%)	25.65 (99%)	25.65 (99%)	25.65 (99%)	25.66 (99%)	25.65 (99%)	25.65 (99%)	25.61 (99%)

302

303

304

305

306

307

308

309

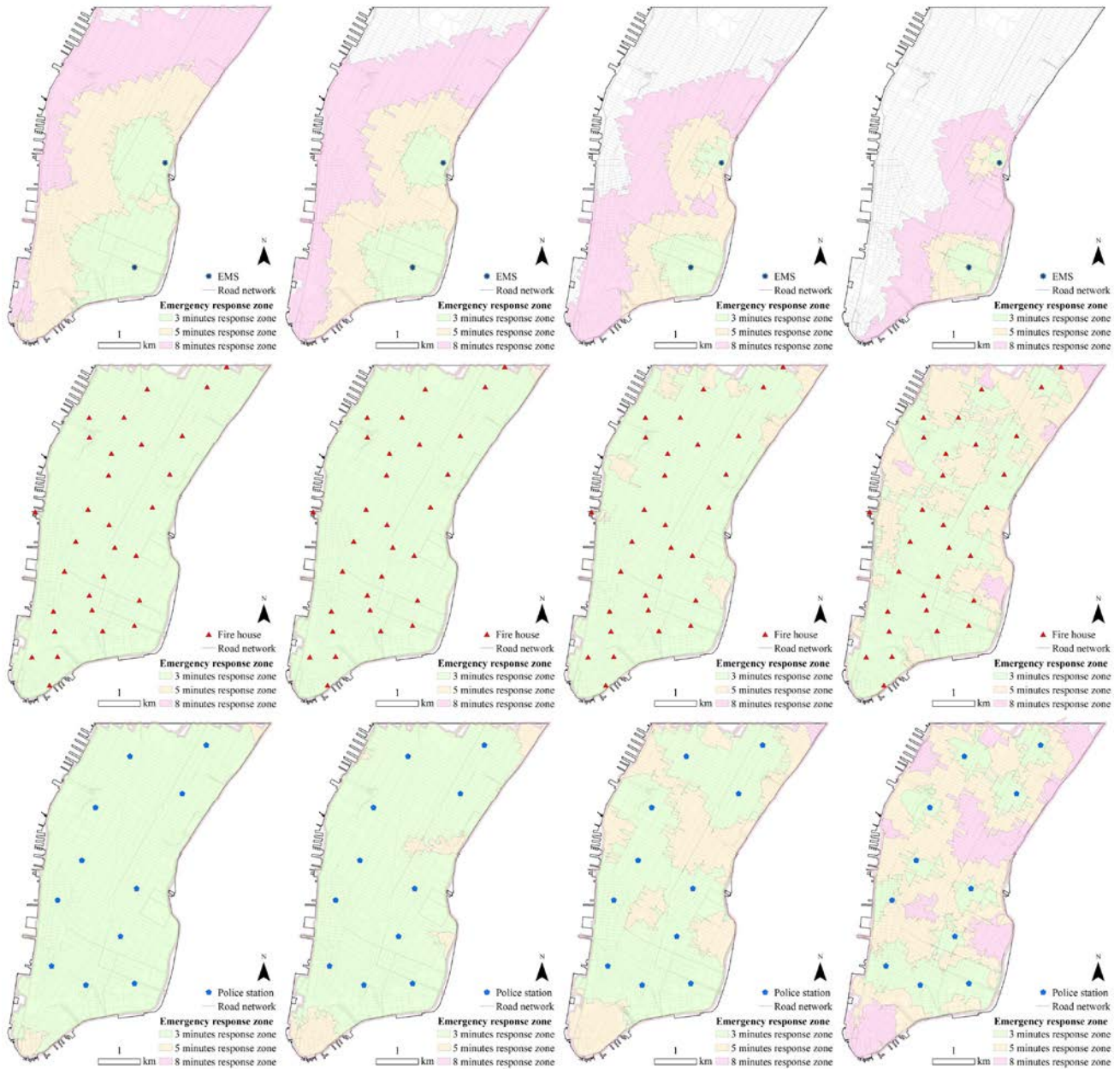
310

311

312

In terms of emergency medical services, the results indicate that, under no flood conditions, spatial coverage of EMS is sensitive to traffic conditions. This is due to the limited number of EMS centers and their uneven distribution (Fig. 3). In Lower Manhattan, there are only two EMS stations that are located in the southern- and mid-eastern parts of the city respectively. Compared to the fire and police services, significantly less coverage is predicted for EMS, especially within the 3- and 5-minute timeframes, with the northwest region most vulnerable. Although 97% of Lower Manhattan would be reachable within 8 minutes or less in unobstructed traffic conditions (e.g. in the evenings), the 8-min EMS response zones cover only 36% of the total area when significant congestion occurs (S4), reducing to 12% and 4% within 5-minute and 3-minute respectively. The results are consistent with the actual EMS response times which were on average 6.39 minutes for life threatening incidents and 9.04 minutes for non-life threatening incidents⁴.

⁴ <http://www.nyc.gov/html/911reporting/html/reports/end-to-end.shtml>



313

314 Fig. 3 Emergency service areas for (3 (green), 5 (yellow), and 8 (pink) -minute timeframes) EMS (upper), Fire houses
 315 (middle) and Police Stations (lower) under normal (no flood) conditions with different travel speeds: S1 in the first column
 316 for S1, S2 in the second column for S2, S3 in the third column for S3, and S4 in the fourth column for S4.

317

318 3.2.2 Emergency services under flood scenarios

319

320 When flood restrictions are incorporated into the network analysis, road disruptions and inaccessible areas can be
 321 identified for each scenario (Table 2). To illustrate such impacts, emergency service areas covered by 3-, 5- and 8-
 322 minute response times with S1 and S4 travel speeds under 100- and 500-year coastal flood scenarios are illustrated
 323 in Fig. 4. The results suggest that coastal flooding exerts varying degrees of impact on the three types of emergency
 324 response coverage. For fire and police services, emergency response can still reach the majority of the area where
 325 the road network has not been disrupted by coastal flooding. This is due to the significant overlaps between service
 326 areas of individual stations, which to a large extent compensate for losses in the coverage by stations directly affected

327 by flooding. In contrast, because of the proximity to shoreline, floodwater directly compromises one of the two EMS
328 centers in all scenarios, leading to a significant reduction (over 30% of the total area) in response coverage to the
329 north of the region. Moreover, a notable 'blind spot' at the island's southern tip can be observed for ambulance and
330 police services under the 2080s flood scenarios due to a lack of in-place facilities and key access routes under
331 floodwater.

332
333 The simulations also show that emergency response service areas gradually decrease with increasing flood magnitude.
334 Around 83% of the total area is reachable in 8 minutes or less by fire and police services under the current 100-year
335 coastal flood event, compared to 75% under the current 500-year scenario. With a 0.76 m rise in sea level projected
336 for 2050s, one police station and two to five fire houses would be directly affected, and 76% and 71% of the road
337 network would be accessible within 8 minutes under 100- and 500-year flood scenarios. When compared with the
338 normal operating conditions, a projected 1.47-m rise in sea level is expected to contribute a 28% to 33% reduction in
339 accessible areas under 100- and 500-year scenarios in 2080s respectively. Up to 37% of Lower Manhattan would be
340 entirely unreachable or 'islanded' for police emergency services under the 500-year scenario in the 2080s, indicating
341 that SLR has significant and non-linear impacts on emergency response spatial accessibility.

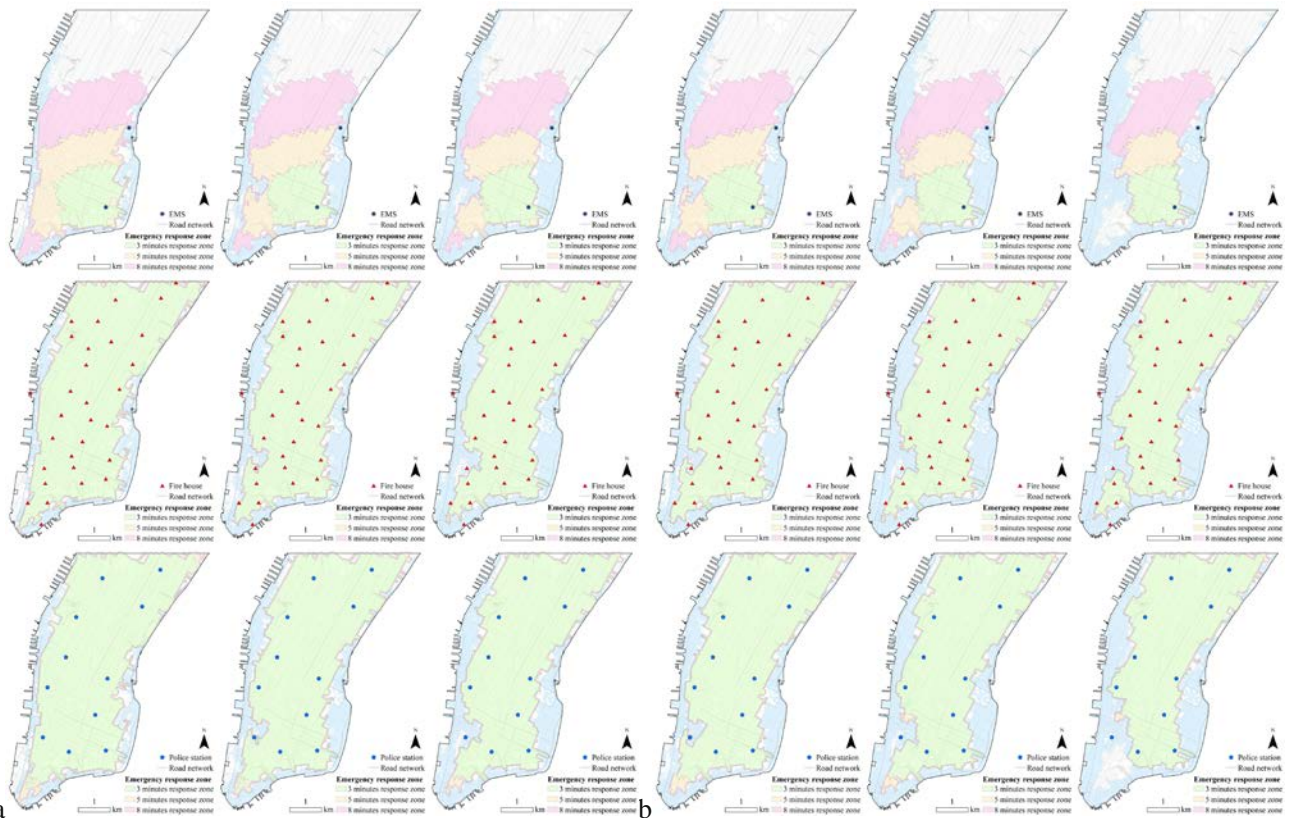
342
343 For the ambulance emergency services, the impact of coastal inundation is more pronounced as only one EMS center
344 would be operational in the flood scenarios. Additionally, the service area is highly sensitive to travel speeds of
345 ambulance vehicles. For example, under normal traffic conditions (i.e. S1), over half (51%) of the area is predicted
346 to be accessible within 8 minutes in the current 100-year flood scenario, compared to 46% under the current 500-
347 year scenario. By contrast, only 15% and 14% of the community can be reached in 8 minutes in congested traffic
348 conditions (i.e. S4) under current 100- and 500-year flood scenarios, respectively. The insensitivity of service to flood
349 magnitude under the same traffic conditions can be explained by the overlaps of EMS spatial coverage between
350 ambulance stations. Furthermore, the impact of SLR on EMS's spatial accessibility for both the 100- and 500-year
351 events demonstrates similar patterns as the fire and police services, with slight decreases in the coverage from present
352 day to 2050s to 2080s. SLR, coastal flood events and the operation of emergency service have different timescales.
353 SLR evolves over decadal and centennial timescales and amplifies storm impact (i.e. duration and/or extent) during
354 period of flood events (days, hours), whilst emergency service responds to coastal flood events that may last hours
355 to days on demand. With the consideration of SLR into discrete points into the near future (2050 and 2080), we
356 investigate how long-term evolution of SLR affects the event-scale emergency responses.

357
358 To investigate the relative impact of SLR on emergency response time, the ambulance response time to healthcare
359 facilities is further quantified via fastest routing under normal and flood scenarios in Lower Manhattan (Fig. 5).
360 Results suggest that compared to normal condition, coastal flooding causes significant increases in response times,
361 mostly due to the lack of access from one EMS and the disruption of coastal highways (e.g. F.D.R). The modelled
362 response time ranges from 0.33 to 8.18 min with an average value of 3.82 min in unobstructed traffic (i.e. S1) under
363 no flood condition, while the average response time increases significantly to 6.18 and 6.19 minutes for the current
364 100y and 500y flood scenarios, respectively. However, SLR exerts a relatively minor impact on EMS response time.
365 For example, with a 1.47 m rise in sea level, ambulance response time on average increases by 0.32 minute for a
366 500y flood event. This can be attributed to the confined nature of flood extents in coastal floodplains.

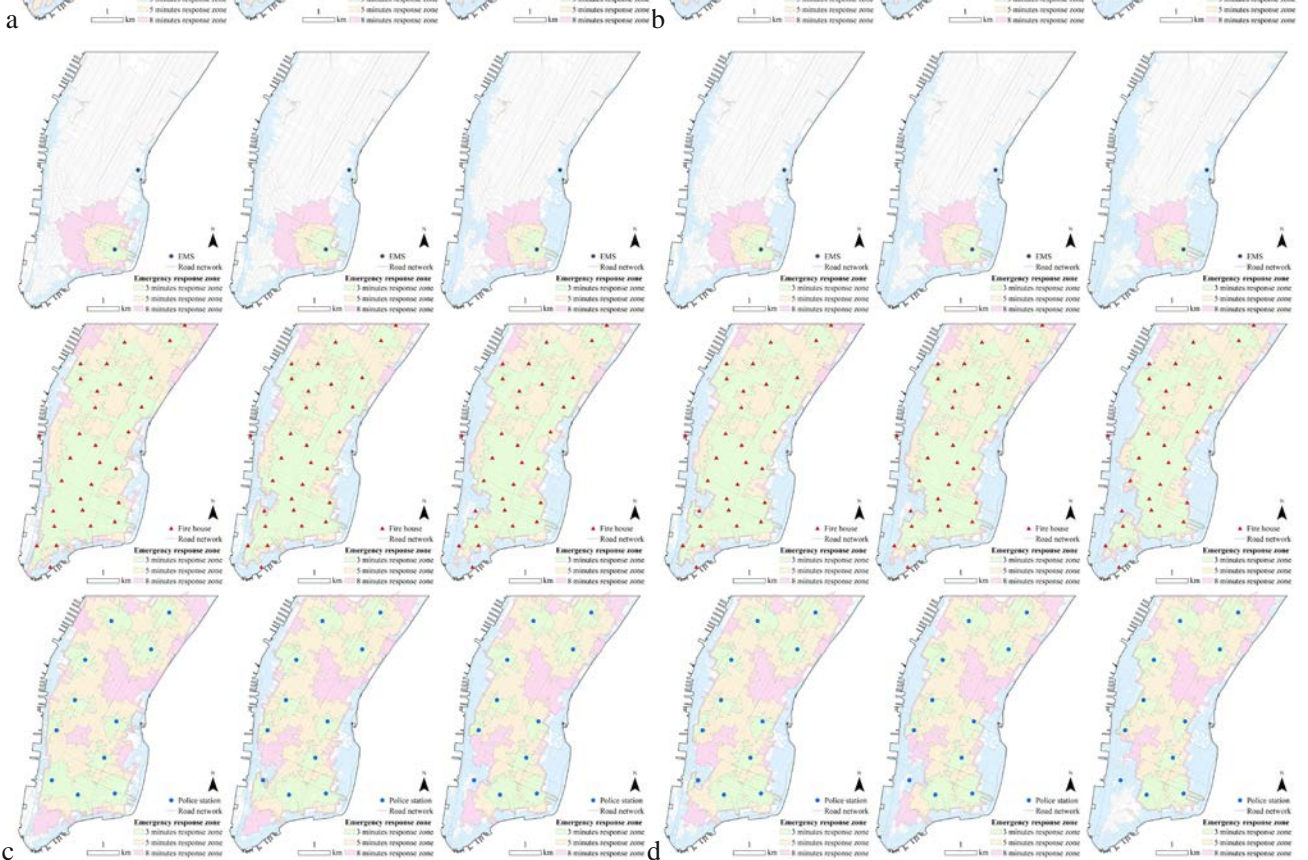
Table 2 Accessibility of emergency services with various travel speeds under flood scenarios in current state, 2050s and 2080s. Unit: km².

Responses with various travel speed	Accessible in current 100- flood scenario			Accessible in current 500- flood scenario			Accessible in 2050s 100- flood scenario			Accessible in 2050s 500- flood scenario			Accessible in 2080s 100- flood scenario			Accessible in 2080s 500- flood scenario		
	3min	5min	8min	3min	5min	8min	3min	5min	8min	3min	5min	8min	3min	5min	8min	3min	5min	8min
EMS-S1	3.19 (12%)	7.52 (29%)	13.35 (51%)	2.83 (11%)	6.58 (25%)	11.87 (46%)	2.86 (11%)	6.73 (26%)	12.11 (47%)	2.66 (10%)	5.75 (22%)	11.09 (43%)	2.71 (10%)	6.07 (23%)	11.3 (43%)	2.48 (10%)	4.49 (17%)	9.05 (35%)
EMS-S2	2.15 (8%)	5.43 (21%)	10.74 (41%)	1.95 (8%)	4.62 (18%)	9.55 (37%)	1.96 (8%)	4.69 (18%)	9.77 (38%)	1.85 (7%)	4.28 (16%)	8.76 (34%)	1.88 (7%)	4.41 (17%)	8.95 (34%)	1.75 (7%)	3.52 (14%)	6.94 (27%)
EMS-S3	1.33 (5%)	3.35 (13%)	7.71 (30%)	1.23 (5%)	2.93 (11%)	6.78 (26%)	1.23 (5%)	2.96 (11%)	6.95 (27%)	1.17 (5%)	2.76 (11%)	6.01 (23%)	1.19 (5%)	2.79 (11%)	6.28 (24%)	1.08 (42%)	2.56 (10%)	4.68 (18%)
EMS-S4	0.65 (3%)	1.65 (6%)	4 (15%)	0.62 (2%)	1.5 (6%)	3.52 (14%)	0.63 (2%)	1.53 (6%)	3.6 (14%)	0.58 (2%)	1.43 (6%)	3.3 (13%)	0.58 (2%)	1.46 (6%)	3.39 (13%)	0.53 (2%)	1.33 (5%)	3.06 (12%)
FDNY-S1	20.07 (77%)	20.66 (79%)	21.51 (83%)	18.19 (70%)	18.74 (72%)	19.51 (75%)	18.4 (71%)	18.96 (73%)	19.76 (76%)	17.27 (66%)	17.81 (69%)	18.57 (71%)	17.52 (67%)	18.06 (69%)	18.83 (72%)	16.09 (62%)	16.65 (64%)	17.44 (67%)
FDNY-S2	19.87 (76%)	20.61 (79%)	21.51 (83%)	18.08 (70%)	18.68 (72%)	19.5 (75%)	18.3 (70%)	18.91 (73%)	19.75 (76%)	17.15 (66%)	17.76 (68%)	18.57 (71%)	17.4 (67%)	18.01 (69%)	18.82 (72%)	15.97 (61%)	16.61 (64%)	17.45 (67%)
FDNY-S3	18.31 (70%)	20.48 (79%)	21.5 (83%)	16.95 (65%)	18.59 (72%)	19.51 (75%)	17.11 (66%)	18.81 (72%)	19.75 (76%)	16.03 (62%)	17.66 (68%)	18.57 (71%)	16.22 (62%)	17.91 (69%)	18.82 (72%)	14.83 (57%)	16.5 (63%)	17.44 (67%)
FDNY-S4	12.05 (46%)	19.41 (75%)	21.51 (83%)	11.2 (43%)	17.9 (69%)	19.5 (75%)	11.34 (44%)	18.07 (70%)	19.75 (76%)	10.56 (41%)	16.95 (65%)	18.57 (71%)	10.71 (41%)	17.18 (66%)	18.82 (72%)	9.56 (37%)	15.75 (61%)	17.45 (67%)
NYPD-S1	19.77 (76%)	20.59 (79%)	21.5 (83%)	17.85 (69%)	18.66 (72%)	19.5 (75%)	18.17 (70%)	18.9 (73%)	19.76 (76%)	16.98 (65%)	17.73 (68%)	18.58 (71%)	17.29 (67%)	17.99 (69%)	18.83 (72%)	15.2 (58%)	15.76 (61%)	16.46 (63%)
NYPD-S2	18.87 (73%)	20.49 (79%)	21.5 (83%)	17.06 (66%)	18.57 (71%)	19.5 (75%)	17.35 (67%)	18.81 (72%)	19.75 (76%)	16.06 (62%)	17.64 (68%)	18.58 (71%)	16.41 (63%)	17.91 (69%)	18.84 (72%)	14.59 (56%)	15.69 (60%)	16.45 (63%)
NYPD-S3	14.27 (55%)	20.11 (77%)	21.5 (83%)	12.76 (49%)	18.27 (70%)	19.59 (75%)	12.9 (50%)	18.51 (71%)	19.75 (76%)	11.96 (46%)	17.3 (67%)	18.58 (71%)	12.03 (46%)	17.61 (68%)	18.84 (72%)	10.9 (42%)	15.52 (60%)	16.49 (63%)
NYPD-S4	6.29 (24%)	16.36 (63%)	21.29 (82%)	5.45 (21%)	14.69 (57%)	19.23 (74%)	5.71 (22%)	14.89 (57%)	19.67 (76%)	5.11 (20%)	13.79 (53%)	18.36 (71%)	5.12 (20%)	13.92 (54%)	18.66 (72%)	4.79 (18%)	12.69 (49%)	16.39 (63%)

2012 2050 2080 2012 2050 2080



370



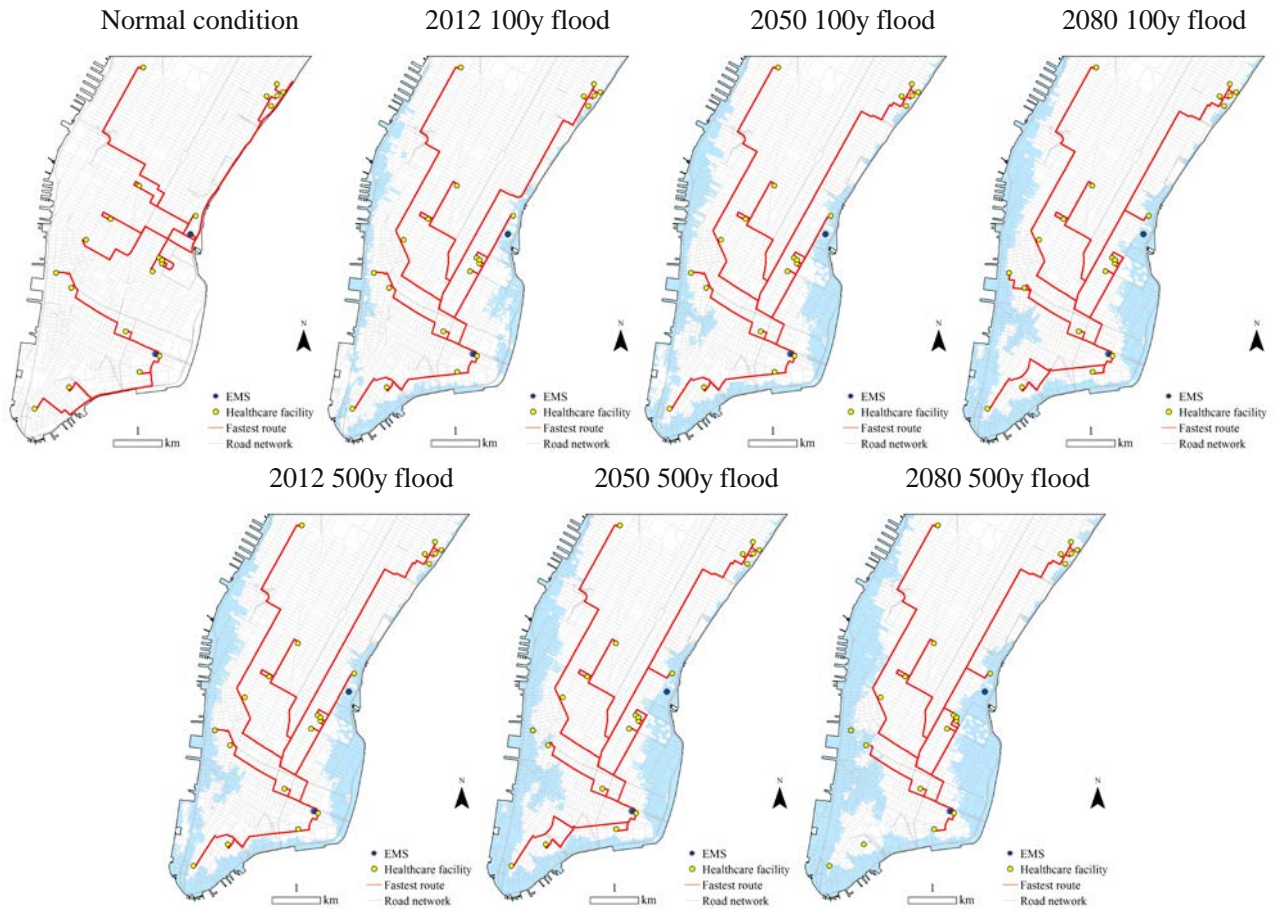
371

372 Fig. 4 Emergency service areas in 3-, 5- and 8-minute response timeframes for EMS, fire houses and police stations under various SLR and coastal flood conditions and different travel speeds: (a) 100-year flood scenarios with S1; (b) 500-year
373 flood scenarios with S1; (c) 100-year flood scenarios with S4; (d) 500-year flood scenarios with S4. Light blue represents
374

375 water depth higher than 50 cm.

376

377



378

379

380

381

Fig. 5 Fastest routes between EMS and healthcare facilities in Lower Manhattan at normal and coastal flood conditions

382

383 3.3 Future perspective and adaptation measures

384

385 Since Lower Manhattan is physically and socio-economically vulnerable to the impacts of SLR and coastal flood
386 events, appropriate resilience measures should be implemented to mitigate the potential negative consequences. As
387 the most effective measure, a coastal flood protective system (BIG U) is likely to be initiated in the next few years to
388 protect the city against SLR and Sandy-like stormwater in the future (Rosenzweig and Solecki, 2014). The project
389 will loop around the entire shoreline of Lower Manhattan with 10 continuous miles of reinforced seawall, stretching
390 from West 57th street south to the Battery and up to East 42th street. The coastal flood defence is designed to
391 withstand a present-day one in 100-year flood plus NPCC's 2050s high-end SLR projection. With this major flood
392 defence system in place, future flood risk and associated impact on emergency responses in the short- to medium-
393 term are expected to be alleviated for this part of the city. However, low probability flood events (i.e. 1 in 100- and
394 1 in 500-year events) may still pose threats to the city over the long term (e.g. 2080s). Hence a new set of approaches
395 (i.e. adaptation pathways) are required to develop sustainable policies and planning which can address the
396 uncertainties from long term change and support flexibility in systems design and management (Deng et al., 2013;
397 Buurman and Babovic, 2016; Manocha and Babovic, 2017).

398

399 In addition to directly tackling SLR and flood hazards, alternative measures can be adopted by emergency services.
400 For example, availability of waterproof vehicles and maneuverable boats which can be easily carried and deployed

401 for storage on a vehicle during coastal flood rescue operations could be one option. Furthermore, emergency service
402 stations could be more strategically positioned to minimize response travel time and maximize spatial coverage with
403 optimal overlap. For example, the EMS center situated in coastal floodplain could be relocated to the middle or north
404 of the region. We also suggest that prepositioning ‘stand-by’ vehicles in predicted ‘blind spots’ as well as establishing
405 temporary facilities (e.g. mobile pumping, demountable floodwall and inflatable bags) at critical nodes or linkages
406 before potential flooding could significantly reduce disruption to emergency services. Moreover, prioritizing the
407 evacuation of vulnerable people (e.g. homebound and elderly residents) and facilities (hospitals and nursing homes)
408 in flood-prone areas would significantly lessen the burden of emergency response during and after a catastrophic
409 flood event.

410

411 **4 Conclusions**

412

413 This study integrated a high resolution 2D hydraulic model (FloodMap) and a widely used GIS spatial analysis tool
414 (Network Analyst) in order to evaluate SLR and coastal flood impacts on emergency service accessibility in Lower
415 Manhattan, NYC. A number of conclusions can be drawn. First, coastal flooding combined with SLR is likely to
416 reduce emergency response spatial coverage and response time via disruption to road network. Second, the
417 performance of emergency services also depends on the station positioning and traffic conditions under both normal
418 and flood scenarios. Finally, even with anticipated strengthening of coastal flood defences in the near future,
419 emergency responders should still be prepared for a potential extreme flood event in a fast changing and uncertain
420 climate. The approach presented here can be readily adopted for applications in other mega- coastal cities such as
421 Shanghai, Mumbai, Bangkok and Jakarta which are particularly vulnerable to SLR and coastal flooding. However,
422 data may not be readily available for developing nations, in particular the integrated transport network (ITN).
423 Methods that adopt simplified ITN in their analysis should be developed for applications in data-sparse situations.

424

425 The analysis provides a detailed analysis of emergency service vulnerability to SLR and coastal flooding, and thus
426 helps to guide decision-making for sustainable coastal flood emergency planning and management. However, to gain
427 more insight and arrive at more robust conclusions, further research is warranted for the following aspects: (i)
428 evaluating the duration, in addition to the spatial coverage of loss of accessibility for emergency services; (ii)
429 incorporating traffic modeling into emergency response assessment to generate more reliable (variable) travel speeds
430 and response times under different scenarios; and (iii) more sophisticated evaluation of network disruption that could
431 take into account velocities as well as depths, and/or severe impedance by debris even in relatively shallow flood
432 waters; and (iv) developing capabilities to forecast accessibility ahead of, during and in the aftermath of coastal flood
433 events to guide operational responses in real-time. Moreover, the present analysis focuses on above ground
434 emergencies, future studies should also be undertaken to assess response times and access to emergencies in
435 flood/partially flooded subways, basements and underground car parks.

436

437 **Acknowledgments** This paper was supported by the National Science Foundation of the United States (Grant no:
438 EAR-1520683), the National Natural Science Foundation of China (Grant no: 41201550) and the Humanities and
439 Social Science Project of Education Ministry of China (Grant no: 17YJAZH111). This research extended work
440 supported by the UK Natural Environment Research Council under the Environmental Risks to Infrastructure
441 Innovation Programme (NE/M008770/1; NE/N013050/1; NE/R009600/1).

442

443 **References**

444 Aerts J C, Botzen W J, Emanuel K, Lin N, de Moel H, Michel-Kerjan E O, 2014. Evaluating flood resilience strategies for

445 coastal mega-cities. *Science*, 344: 473-475.

446 Bates P D, Dawson R J, Hall J W, Horritt M S, Nicholls R J, Wicks J, Hassan M A A M, 2005. Simplified two-dimensional
447 numerical modelling of coastal flooding and example applications. *Coastal Engineering*, 52: 793-810.

448 Bates P D, Horritt M, Fewtrell T, 2010. A simple inertial formulation of the shallow water equations for efficient two-
449 dimensional flood inundation modelling. *Journal of Hydrology*, 387: 33-45.

450 Blumberg A, Georgas N, Yin L, Herrington T, Orton P, 2015. Street Scale Modeling of Storm Surge Inundation along the
451 New Jersey Hudson River Waterfront. *Journal of Atmospheric and Oceanic Technology*, doi:10.1175/JTECH-D-14-
452 00213.1.

453 Buurman J, Babovic V, 2016. Adaptation Pathways and Real Options Analysis: An approach to deep uncertainty in climate
454 change adaptation policies. *Policy and Society*, 35 (2): 137-150.

455 Chang H, Lafrenz M, Jung I, Figliozzi M, Platman D, Pederson C, 2010. Potential impacts of climate change on flood-
456 induced travel disruptions: a case study of Portland, Oregon, USA. *Annals of the Association of American*
457 *Geographers*, 100: 1-14.

458 Coles D, Yu D, Wilby R L, Green D, Herring Z, 2017. Modelling emergency service accessibility during flooding in York,
459 UK, *Journal of Hydrology*, 546: 419-436.

460 Colle B A, Buonaiuto F, Bowman M J, Wilson R E, Flood R, Hunter R, Mintz A, Hill D, 2008. New York City's
461 vulnerability to coastal flooding. *Bulletin of the American Meteorological Society*, 89: 829-841.

462 Deng Y, Cardin M, Babovic V, Santhanakrishnan D, Schmitter P, Meshgi A, 2013. Valuing flexibilities in the design of
463 urban water management systems. *Water research*, 47 (20): 7162-7174.

464 Fewtrell T, Bates P D, Horritt M, Hunter N, 2008. Evaluating the effect of scale in flood inundation modelling in urban
465 environments. *Hydrological Processes*, 22: 5107-5118.

466 Engelhart S E, Horton B P, 2012. Holocene sea level database for the Atlantic coast of the United States. *Quaternary*
467 *Science Reviews*, 54: 12-25.

468 Federal Emergency Management Agency, 2013. Flood insurance study: City of New York.

469 Gil J, Steinbach P, 2008. From flood risk to indirect flood impact: evaluation of street network performance for effective
470 management, response and repair. in Proverbs D, Brebbia C A, Penning-Roswell E (eds.) *Flood Recovery, Innovation*
471 *and Response (FRIAR 2008)*, Wessex Institute of Technology Press, UK, 335-345.

472 Green, D., Yu, D., Pattison, I., Wilby, R., Boshier, L., Patel, R., Thompson, P., Trowell, K., Draycon, J., Halse, M., Yang,
473 L., and Ryley, T. (2017). City-scale accessibility of emergency responders operating during flood events, *Nat. Hazards*
474 *Earth Syst. Sci.*, 17, 1-16, doi:10.5194/nhess-17-1-2017.

475 Hallegatte S, Green C, Nicholls R J, Corfee-Morlot J, 2013. Future flood losses in major coastal cities. *Nature Climate*
476 *Change*, 3: 802-806.

477 Hay C C, Morrow E, Kopp R E, Mitrovica J X, 2015. Probabilistic reanalysis of twentieth-century sea-level rise. *Nature*,
478 517: 481-484.

479 Horton R, Little C, Gornitz V, Bader D, Oppenheimer M, 2015. New York City Panel on Climate Change 2015 Report
480 Chapter 2: Sea Level Rise and Coastal Storms. *Annals of the New York Academy of Sciences*, 1336: 36-44.

481 Hu A, Deser C, 2012. Uncertainty in future regional sea level rise due to internal climate variability. *Geophysical Research*
482 *Letters*, 40: 2768-2772.

483 IPCC, 2012. *Climate Change 2012: The Physical Science Basis*. Cambridge University Press, Cambridge.

484 Kopp R E, Horton R M, Little C M, Mitrovica J X, Oppenheimer M, Rasmussen D J, Strauss B H, Tebaldi C, 2014.
485 Probabilistic 21st and 22nd century sea level projections at a global network of tide gauge sites. *Earth's Future*, 2:
486 383-406.

487 Kreibich H, Piroth K, Seifert I, Maiwald H, Kunert U, Schwarz J, Merz B, Thielen A H, 2009. Is flow velocity a significant
488 parameter in flood damage modelling? *Natural Hazards and Earth System Sciences*, 9: 1679-1692.

489 Levermann A, Griesel A, Hofmann M, Montoya M, Rahmstorf S, 2005. Dynamic sea level changes following changes in
490 the thermohaline circulation. *Climate Dynamics*, 24(4): 347–354.

491 Manocha N, Babovic V, 2017. Development and valuation of adaptation pathways for storm water management
492 infrastructure, *Environmental Science & Policy*, 77: 86-97.

493 Mitrovica J X, Tamisiea M E, Davis J L, Milne G A, 2001. Recent mass balance of polar ice sheets inferred from patterns
494 of global sea-level change. *Nature*, 409: 1026-1029.

495 Neal J C, Schumann G, Fewtrell T, Budimir M, Bates P, Mason D, 2011. Evaluating a new LISFLOOD-FP formulation
496 using data for the summer 2007 floods in Tewkesbury, UK. *Journal of Flood Risk Management*, 4(2): 88-95.

497 Nicholls R J, Cazenave A, 2010. Sea-level rise and its impacts on coastal zones. *Science*, 328: 1517–1520.

498 Lin N, Emanuel K Oppenheimer M, Vanmarcke E, 2012. Physically based assessment of hurricane surge threat under
499 climate change. *Nature Climate Change*, 2(6): 462-467.

500 Lin N, Kopp R E, Horton B P, Donnelly J P, 2016. Hurricane Sandy’s flood frequency increasing from year 1800 to 2100.
501 *Proceedings of the National Academy of Sciences*, doi: 10.1073/pnas.1604386113.

502 NYC Department of Transportation, 2016. 2016 New York City Mobility Report. New York City, NY, USA.

503 NPCC2 Climate Risk Information, 2013. Climate Methods Memorandum. New York City Council, Available at:
504 [http://www.nyc.gov/html/planyc2030/downloads/pdf/NPCC2_Climate%20Methods%20Memorandum_2013.pdf?ep](http://www.nyc.gov/html/planyc2030/downloads/pdf/NPCC2_Climate%20Methods%20Memorandum_2013.pdf?epi-content=GENERIC)
505 [i-content=GENERIC](http://www.nyc.gov/html/planyc2030/downloads/pdf/NPCC2_Climate%20Methods%20Memorandum_2013.pdf?epi-content=GENERIC)

506 NYC Mayor’s Office, 2012. NYC Hurricane Sandy After Action: Report and Recommendations to Mayor Michael R.
507 Bloomberg. New York City, NY, USA.

508 NYC Office of Emergency Management, 2014. 2014 New York City Hazard Mitigation Plan. New York City, NY, USA.

509 Peltier W R, 2004. Global glacial isostasy and the surface of the ice-age Earth: The ICE-5G (VM2) model and GRACE.
510 *Annual Review of Earth and Planetary Sciences*, 32: 111-149.

511 Ramirez J A, Lichter M, Coulthard T J, Skinner C, 2016. Hyper-resolution mapping of regional storm surge and tide
512 flooding: comparison of static and dynamic models. *Natural Hazards*, doi:10.1007/s11069-016-2198-z.

513 Rosenzweig C, Solecki W, 2014. Hurricane Sandy and adaptation pathways in New York: Lessons from a first-responder
514 city. *Global Environmental Change*, 28: 395-408.

515 Schubert J E, Sanders B F, 2012. Building treatments for urban flood inundation models and implications for predictive
516 skill and modeling efficiency. *Advances in Water Resources*, 41: 49-64.

517 Talke S A, Orton P, Jay D A, 2014. Increasing storm tides at New York City, 1844-2012. *Geophysical Research Letters*,
518 41: 3149-3155.

519 Tingsanchali T, 1996. Floods and human interaction: experiences, problems, and solutions, report. Asian Institute of
520 Technology, Bangkok, Thailand.

521 Wang H V, Loftis J D, Liu Z, Forrest D, Zhang J, 2014. The Storm Surge and Sub-Grid Inundation Modeling in New York
522 City during Hurricane Sandy. *Journal of Marine Science and Engineering*, 2: 226-246.

523 Yin J, Yu D, Yin Z, Liu M, He Q, 2016. Evaluating the impact and risk of pluvial flash flood on intra-urban road network:
524 a case study in the city center of Shanghai, China. *Journal of Hydrology*, 537: 138-145.

525 Yin J, Lin N, Yu D, 2016. Coupled modeling of storm surge and coastal inundation: a case study in New York City during
526 Hurricane Sandy. *Water Resources Research* 52: 8685-8699.

527 Yu D, Lane S N, 2006a. Urban fluvial flood modelling using a two-dimensional diffusion wave treatment, part 1: mesh
528 resolution effects. *Hydrological Processes*, 20: 1541-1565.

529 Yu D, Lane S N, 2006b. Urban fluvial flood modelling using a two-dimensional diffusion wave treatment, part 2:
530 development of a sub grid-scale treatment. *Hydrological Processes*, 20: 1567-1583.

531 Yu D, Lane S N, 2011. Interaction between subgrid-scale resolution, feature representation and grid-scale resolution in
532 flood inundation modelling. *Hydrological Processes*, 25: 36-53.